EXPLOITING GOME AND ATSR-2 DATA: FIRST RESULTS OF THE PAGODA PROJECT

Thomas Popp
Gerhard Gesell
Thomas K&oumlnig
Deutsche Forschungsanstalt f&uumlr Luft- und Raumfahrt (DLR)
Deutsches Fernerkundungsdatenzentrum (DFD)
Oberpfaffenhofen
82234 We&szligling
Germany
Phone +49-8153-28 2672
FAX +49-8153-28 1420
e-mail: Prename.Name@dlr.de
URL: http://www.dfd.dlr.de/de

Theo Kriebel
Ralf Meerk&oumltter
Hermann Mannstein
Deutsche Forschungsanstalt f&uumlr Luft- und Raumfahrt (DLR)
Institut f&uumlr Physik der Atmosph&aumlre
Oberpfaffenhofen
82234 We&szligling
Germany
Phone +49-8153-28 2537
FAX +49-8153-28 1841
e-mail: Prename.Name@dlr.de

ABSTRACT

This paper presents first results of the AO2-Project for GOME and ATSR-2 Data Application (PAGODA) which exploits simultaneous measurements of the sensors GOME and ATSR-2. The spatial resolution of ATSR-2 which is much better than that of GOME toge-ther with its biangular observation allows to estimate the predominant cloud and surface signal. This is a prerequisite for analysing the spectral information of GOME to retrieve aerosol parameters and surface UV-B radiation.

Cloud parameters inside a GOME pixel are calculated from collocated ATSR-2 pixels by use of the adapted APOLLO (AVHRR Processing scheme Over cLouds, Land and Ocean) software. For cloudfree pixels the boundary layer aerosol type over land is deduced with a new method: A dark field technique yields aerosol optical depth and surface albedo from visible/near infrared ATSR-2 data. Subsequently, the comparison of simulated radiances with measured GOME spectra gives the aerosol mixture. By use of GOME ozone column amounts and ATSR-2 cloud/aerosol optical depths horizontal distributions of the erythemally weighted surface UV-B irradiances are calculated.

An application of these methods to one test case demonstrates the potential of the PAGODA multisensor retrieval approaches.

Keywords: GOME, ATSR-2, clouds, aerosol, UV-B

1. INTRODUCTION

Understanding climate change and predicting its consequences requires insight into a number of fundamental processes and knowledge about the distribution and trends of a set of key species. Whereas some of these are quite well-known (e.g. inert trace gases, IPCC 1995) the knowledge about others is very uncertain. One major deficiency lies in the role of clouds and aerosols (IPCC 1992, 1995; Cess *et al.*1995), their interaction and their impact on atmospheric radiance and on the harmful UV-B radiation. To enhance the monitoring capacity of satellite remote sensing the project PAGODA (Project for GOME and ATSR-2 Data Application, Schlichter *et al.* 1994) has been started within a DLR program on atmospheric remote sensing.

The focus of this project lies in the development of new methods for the retrieval of geophysical parameters by exploiting simultaneous measurements of the two sensors GOME (Global Ozone Monitoring Experiment) and ATSR-2 (Along Track Scanning Radiometer 2), both onboard the polar orbiting European Space Agency's satellite ERS-2 (European Research Satellite 2) which has been launched on April 21, 1995. Whereas the grating spectrometer GOME measuring spectra in the range from 240-790 nm gives a spatial re-solution of 40x40 km2 to 320x40 km2, the conical scan of the ATSR-2 radiometer measures nadir and forward reflectances in 4 solar and 3 thermal channels in a much finer resolution of about 1x1 km2. Beyond the subjects described in this paper the PAGODA project deals with the retrieval of polar stratospheric clouds, the validation of the coupled dynamic-chemical circulation model ECHAM/CHEM, the retrieval of sea ice contamination, the treatment of nonspherical scattering, the comparison of GOME and ATSR-2 cloud cover estimation and of GOME and POLDER polarization.

Clouds strongly influence the radiative energy balance of the atmosphere: clouds contribute most to the Earth's shortwave albedo, while redusing the longwave radiation escaping into space (e.g., Ramanathan *et al.* 1989; Arking 1991). However, not much is known yet about the exact climate influence of clouds. For example, the main difference between climate models is their treatment of clouds (Cess *et al.* 1989). Because clouds are very variable in space and time, satellite measurements are indispensable. Another aspect of clouds is that they are a severe problem for retrieval of trace gases and aerosols from spectral satellite observations at low spatial resolution (e.g. accurate ozone column and profile retrievals from GOME data depend on a reliable cloud detection method).

Aerosols have a direct effect on the atmospheric albedo by scattering and absorption (e. g. Kaufman *et al.* 1991), but also an indirect effect because they initiate and alter cloud formation in the presence of water vapour (e.g. Hansen and Lacis 1990; Charlson *et al.* 1992). Aerosols in the troposphere are transported over very long distances, thus contributing to the disper-sal of pollution on global scales. In addition, aerosols are involved in chemical reactions in the atmosphere and thus affect the transformation of climatologically and environmentally important species. Furthermore, aerosols mean a strong uncertainty for optical remote sensing of surfaces.

The worldwide ozone depletion observed in recent decades (e.g. Stolarski *et al.* 1991; World Meteorological Organization 1995), the expected minimum of ozone concentration in the early next century and subsequent increasing UV radiation levels at the surface (Blumthaler and Ambach 1990; Herman *et al.* 1996; Madronich *et al.* 1992) have inspired the development of methods for monitoring surface UV-B radiation via satellite. Since the increase of UV-B radiation at the surface is related to harmful effects on human health, aquatic and terrestrial ecosystems and production of crops (Armstrong 1993; Caldwell and Flint 1993; De Fabo and Noonan 1993; Smith 1993) satellite remote sensing techniques are of interest and may supplement surface measurements in order to achieve more comprehensive global information about this important environmental parameter.

Currently no complete observations of cloud and aerosol characteristics are available. Researchers have to rely on rare and expensive in situ measurements and climatological datasets. The only operational retrieval methods from satellite measurements

(clouds: ISCCP climatology; aerosols: NOAA optical depth, Rao, *et al.* 1989) are li-mited in their coverage (aerosol only over oceans) and content (clouds: no vertical structure; aerosol: only column optical depth). Therefore the development of operational methods to extract multiparameter information on clouds and aerosols is a high priority of international climate change research (e.g. aerosol focus in IGBP core project IGAC). Clearly, the manifold interactions between clouds and aerosols require, if possible, simultaneous observations using satellite instruments (e.g. King *et al.* 1992).

Trend estimates of surface UV-B based on satellite data have been performed by Herman *et al.* (1996) and Madronich *et al.* (1992) who use TOMS data and by Lubin and Jensen (1995) who combined TOMS with ERBE (Earth-Radiation-Budget-Experiment) data. Whereas direct long-term surface measurements of UV-B show disparate trends probably depending on local pollution or cloudiness and the altitude above sea level (e.g. Blumthaler and Ambach 1990; Correl *et al.* 1992) the satellite data analysis gives an increase of UV-B, at least for mid- and high-latitude belts.

It is the aim of this paper to present new methods for cloud detection, aerosol retrieval and the calculation of the surface UV-B radiation by the combined usage of the two different satellite instruments GOME and ATSR-2 onboard ERS-2.

2. DESCRIPTION OF METHODS

2.1. Cloud Detection

The APOLLO software (Saunders and Kriebel 1988; Gesell 1989; Kriebel *et al.* 1989) has been successfully extended for dealing with ATSR-2/SADIST data. Gridded reflectances and temperatures in those ATSR-2 channels which are equivalent to the AVHRR's spectral bands are used for cloud detection; the 1.6 mm channel is used to separate clouds from snow.

In a first run five algorithms, two in the solar spectral range, three in the thermal infrared, decide if a pixel is cloudfree or not. In a second run two of the algorithms check the pixels detected as not cloudfree for total cove-rage or not. The algorithms are based on different physical principles and are therefore sensitive to different types of clouds. They add their results up into a cloud mask which can afterwards be cleared from cloudfree snow pixels using the 1.6 mm channel.

An IR-"Gross" test simply determines pixels to be cloud contaminated if they are colder then a threshold in channel 5. A spatial coherence test looks for scattered clouds by checking the local temperature variance. The diffe-rence of temperatures in channels 4 and 5 is sensitive for thin cirrus clouds. This test takes dependence of the thresholds on temperature and relative atmosphere into account. The dynamic visible and dynamic ratio algorithms check reflectances and reflectance ratios of solar channels 1 and 2 using thresholds which are adjusted dynamically by local histograms. Cloud contaminated pixels will be flagged as totally covered if the spatial coherence test finds the local temperature variance to be low and/or the dynamic ratio test finds the pixel's reflectance ratio close to the cloud peak value of the histogram.

After calculation of the cloud mask cloud optical thicknesses are derived from channel 1 (0.67 mm) reflectances by means of a parametrization scheme. Partially cloud filled pixels are treated as cloud free pixels in this study. However, an appropriate parametrization for these pixels is under development.

2.2. Aerosol Retrieval

Aerosol parameters are retrieved from a combination of simultaneous ATSR-2 and GOME data. The main new result is an estimation of the type of aerosol in the boundary layer over land. The treatment of ATSR-2 data is based on an extended version of the atmospheric correction software EXACT (Popp 1993 and 1995) which has been validated with Landsat-TM and NOAA-AVHRR data. Thus aerosol and surface characteristics can be estimated for cloudfree pixels: With a dark field method total optical depths and the bispectral wavelength index are derived for automatically selected dark targets (dark forest, water bodies). This algorithm uses all 6 visible/near infrared forward and nadir reflectances from the gridded brigthness temperature/reflectance product (GBT). Then the atmospheric correction yields surface albedo values for the 3 wavelengths 560, 670 and 870 nm. The wavelength index and the agreement of nadir/forward optical depths give a first indication of the type of aerosol.

These ATSR-2 derived data are then colocated to GOME pixels and interpolated spectrally. Using the calculated optical depths and surface albedo values, GOME spectra for a set of 40 aerosol mixtures are simulated with an ite-rative code (successive orders of scattering, SOS; Nagel *et al.* 1978) which includes full multiple scattering. For the modelling of aerosols the external mixing approach (WCP 1986) based on 9 components from the OPAC database (Optical properties of aerosols and cloudss, Hess 1997) and the LOWTRAN7 (Kneizys *et al.* 1988) models are used in the boundary layer. For humidity dependent components two models with 50% and 95% relative humidity have been included. Further, a fresh and aged volcanic type in the stratosphere have been included.

In the current test version these spectra are calculated at 20 wavelenghts which are free of severe instrument errors (e.g. noise in band overlap regions) and gas absorption lines. The broad ozone absorption in the Chappuis band is corrected utilizing GOME retrieved ozone columns (level 2 product). For a fast application precalculated radiative transfer results have been stored in a large database. A least square fit of the simulations to the measured GOME spectrum (level 1 product) results in the selection of the most plausible type of aerosol in a GOME pixel. The use of reflectance values obtained from onboard solar irradiance measurements for both instruments reduces calibration errors significantly as compared to the use of calibrated radiances.

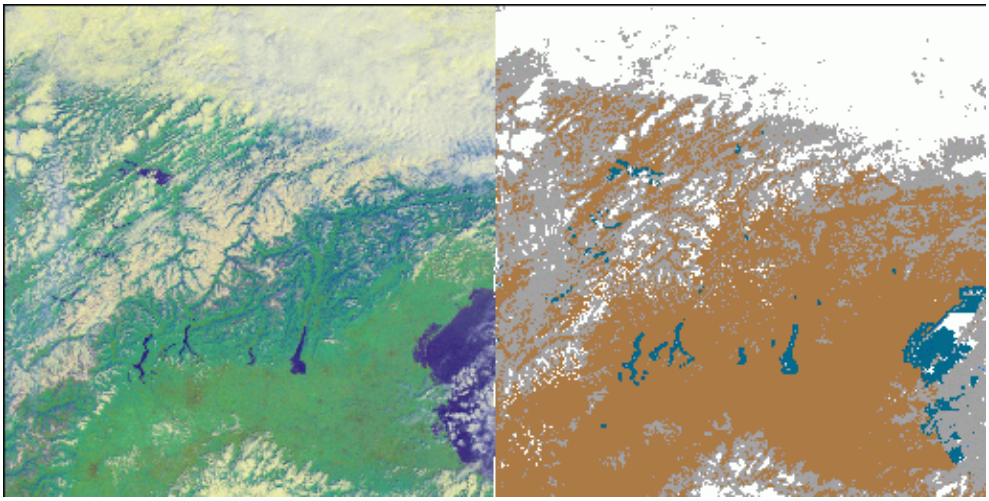

Figure 1: ATSR-2 frame 2655 of orbit 1922 on 2.9.95. Left: RGB nadir image (channels 0.67, 0.87, 12.0 mm). Right: Cloud mask with cloudfree land (brown) and sea (blue), partially (grey) and fully (white) cloudy pixels.

2.3. UV-B Calculation

In principle the UV-B irradiance at the surface is calculated indirectly by using actual satellite measurements of the main UV-B affecting atmospheric parameters as input for a data base which contains the results of radiative transfer calculations for various atmospheric conditions. The UV-B affecting parameters which were varied in these calculations are: solar zenith angle (20-75°), ozone column (200-400 Dobson units), and cloud optical thickness (0-120). For the other UV-B affecting parameters the present version assumes constant values: aerosol optical depth 0.2, and surface albedo 0.03 (surface is not covered with snow in summer). The data base accounts for surface altitudes of 0, 250, 500, 750 and 1000 m above sea level. Model clouds have been embedded between 2.5 and 4.5 km, the meteorological parameters correspond to those of the standard atmosphere 'midlatitude summer'.

The UV-B data base has been generated with a radiative transfer model based on the matrix-operator-theory (Plass *et al.* 1973). This model accounts for multiple scattering and absorption processes on air molecules, aerosol/cloud particles and ozone in the spectral range from 290-320 nm with a spectral resolution of 0.5 nm. Spatial distributions of UV-B irradiances at the surface are then obtained with a program that relates satellite measured cloud optical depths (see 3.1.) and ozone column amounts (GOME level 2 product) to model calculated UV-B spectra. It multiplies them with the CIE response spectrum (McKinlay and Diffey 1987) and finally attaches wavelength integrated and erythemal weighted UV-B irradiance to ATSR-2 pixels accounting for the actual solar zenith angle of each pixel. The UV-B data base converts cloud optical thicknesses in the visible to those in the UV-B spectral range.

3. FIRST RESULTS

3.1. Cloud Detection

Figure 1 shows the result of the APOLLO cloud detection scheme applied to an ATSR-2 frame (orbit 1922, frame 2655) of the central Alpine region on September 2nd, 1995. A color composit of the nadir channels at 0.67 mm, 0.87 mm and 12.0 mm on RGB (left) shows lake Konstanz, the Italian lakes and the Golf of Venice in dark blue color. The result of the cloud detection (right) includes an additional correction for errors due to snow coverage. Brown and blue colors indicate cloudfree land and sea areas, respectively. Totally cloud covered pixels appear in white, grey colored pixels have been classified to be neither cloudfree nor totally cloud covered.

Distributions of the cloud optical thicknesses on 2. September are given in figure 4 which displays 5x5 pixel averages in a range up to a value of 139. As shown, the area of the Po basin South of the Alps appears to be mostly cloudfree, whereas clouds are found in Southern Germany and Austria.

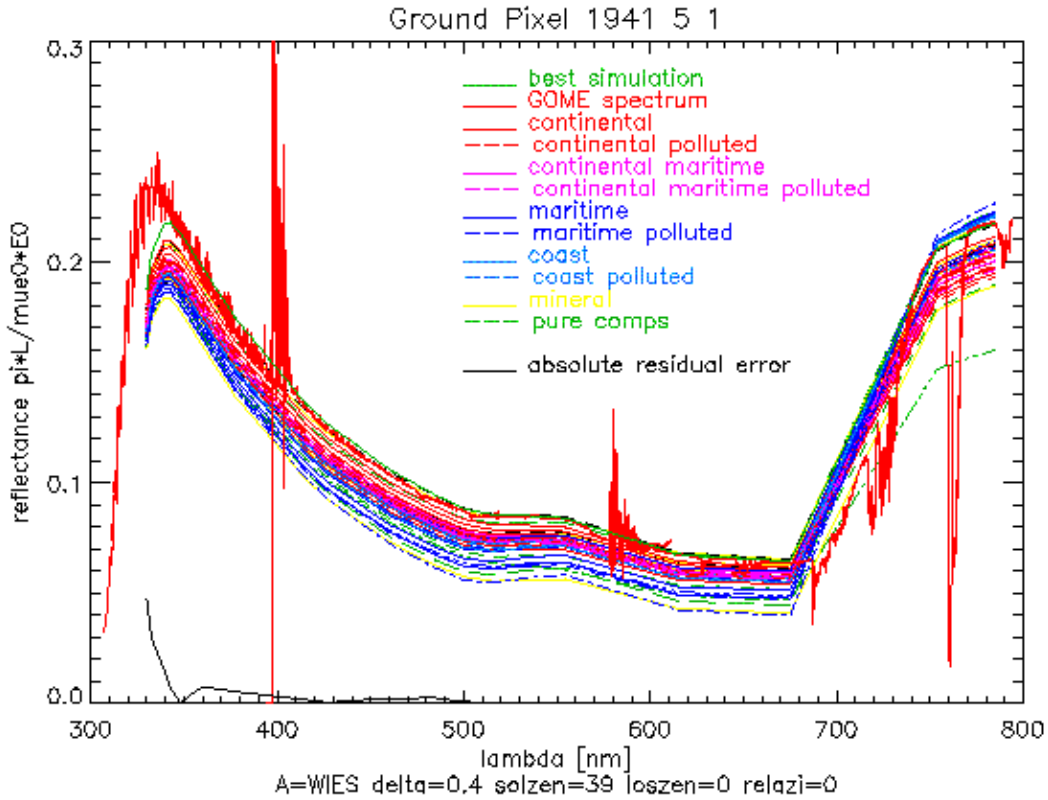

Figure 2: GOME pixel 1941 of orbit 1921 on 2.5.95. Simulated spectra for 40 aerosol mixes. All simulations calculated with total optical depths and surface albedos derived from colocated ATSR-2 pixels.

3.2. Aerosol Retrieval

For the same ATSR-2 frame as in section 3.1. the aerosol algorithm has been applied yielding colocated results for GOME pixels with low cloud cover. As a first demonstration of the aerosol retrieval GOME nadir pixel number 1941 (center coordinates: latitude 45.77°, longitude 8.63°) of commissioning phase orbit 1921 (corresponds to ATSR-2 orbit 1922 above 42° Northern latitude) with a size of 80x40 km2 located around the South edge of Lago Maggiore has been selected. The APOLLO derived a total cloud cover of 4% within the GOME pixel. The ATSR-2 aerosol algorithm delivered a total optical depth of 0.40 at 550 nm wavelength using 234 cloudfree dark ATSR-2 pixels. This comprises of 0.10 Rayleigh optical depth, 0.04 above boundary layer aerosol optical depth, and 0.26 boundary layer aerosol optical depth. The atmosphere corrected surface albedos were calculated as 0.065, 0.055, 0.332 at 560, 670, 870 nm, respectively. The wavelength index was calculated to be 1.02 from the green and red channels' boundary

layer aerosol optical depths; out of the 4 LOWTRAN7 components the rural model fitted best in nadir and forward retrieval. From the atmosphere corrected vegetation index of 0.726 a pasture land surface type was selected and adjusted with the retrieved surface albedo values at the 3 ATSR-2 wavelengths. The solar zenith angle at the pixel center was 39°.

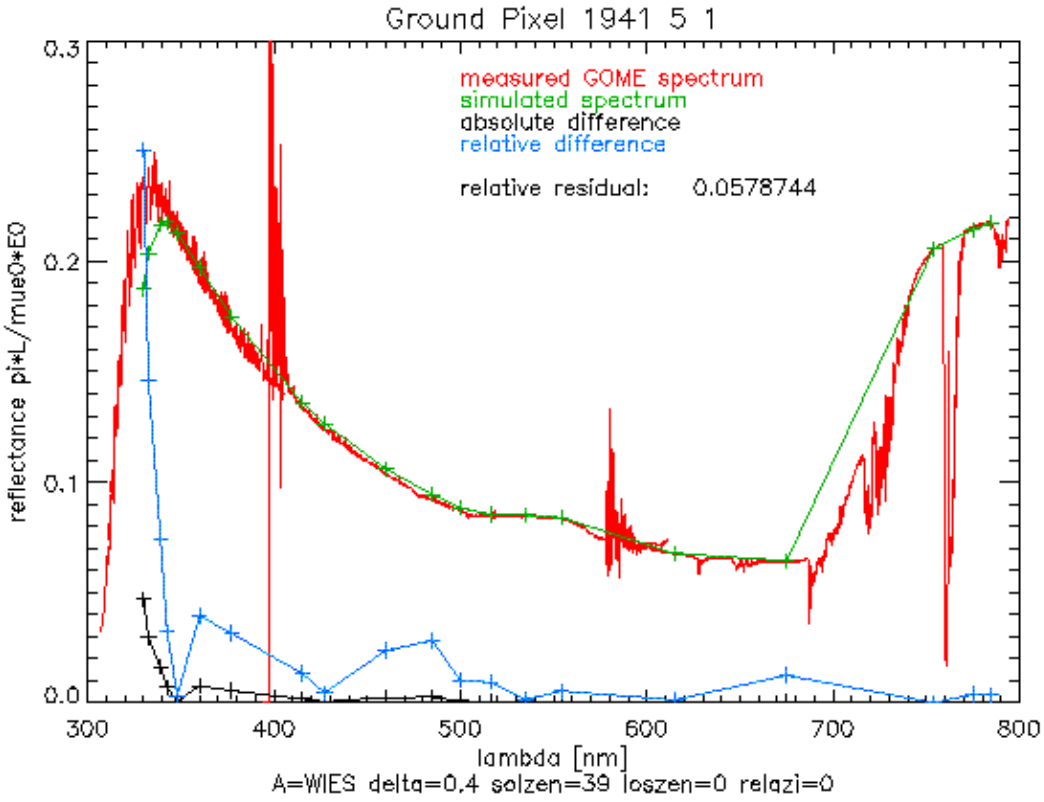

Figure 3: GOME pixel 1941 of orbit 1921 on 2.5.95. Best fit with error. All simulations calculated with total optical depths and surface albedos derived from colocated ATSR-2 pixels.

Figure 2 shows the 40 simulated cloudfree spectra. The difference in absolute values and derivatives of the different mixtures can be seen clearly. Out of these simulated spectra the least square fit selected a low humidity (50%) pure water soluble component with a relative residual of 0.058. The mixtures closest to this best choice were unpolluted continental mixtures of the insoluble/dustlike and water soluble components with a high percentage of the water soluble component, but also the pure sea salt (accumulation mode), mineral (nucleation mode) and aged volcanic (stratospheric optical depth increased to 0.1) models. Maritime mixtures as well as all soot-polluted mixtures were clearly separated. The selected unpolluted continental type of aerosol is plausible as the weather situation on 2nd September 1995 in Central Europe was characterised by predominantly North-Westerly winds. However, as the results of this first demonstration indicate a further sensitivity/error analysis is necessary to define unresolvable ambiguities in the aerosol type retrieval depending on the aerosol optical depth. The selected simulated and the measured spectrum together with the absolute and relative residual are also shown in figure 3. The crosses indicate the 20 wavelengths selected for the simulations. The figure shows a good agreement except below 350 nm which explains the unsatisfactory residual of 0.058. Since it is intended to use this wavelength region for an estimation of the vertical aerosol layering a further investigation in this large difference needs to be done.

3.3. UV-B Calculation

Horizontal distributions of erythemal weighted UV-B irradiances corresponding to the distribution of the cloud optical thickness (figure 4) are presented in figure 5. The ozone column amount as measured by GOME in its pixel number 1941 and underlying this UV-B map is 298.4 Dobson units. Due to a rather flat surface topography within the region of interest directly located South of the Alps a surface altitude of 250 m above sea level has been used for the calculation of surface UV-B irradiances in the whole test area. Thus, derived irradiance values are not realistic in the Alpine region and over Southern Germany. In a next step a digital elevation model will account for the influence of topography on surface UV-B.

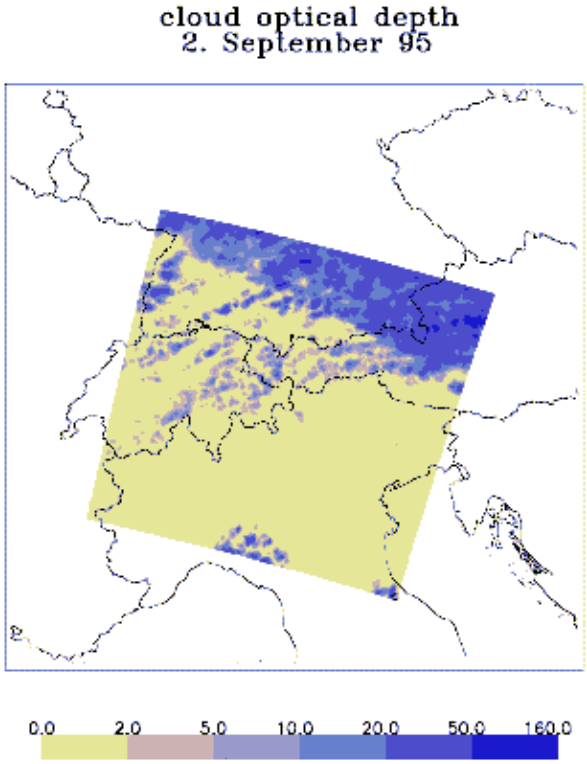

Figure 4: Cloud optical depth on 2. 9. 1995 derived with APOLLO.

Figure 5 shows irradiances varying in a range from about 15 mWm-2 to 131 mWm-2 with the maximum va-lues inside the cloudfree Po basin. As a qualitative result it can be seen that UV-B irradiances decrease in regions where cloud optical thickness increases. This demonstrates how the method accounts for the influence of clouds in the ATSR-2 resolution, i.e. the sub-pixel resolution of GOME. Variations of the aerosol optical depth have not yet been taken into account.

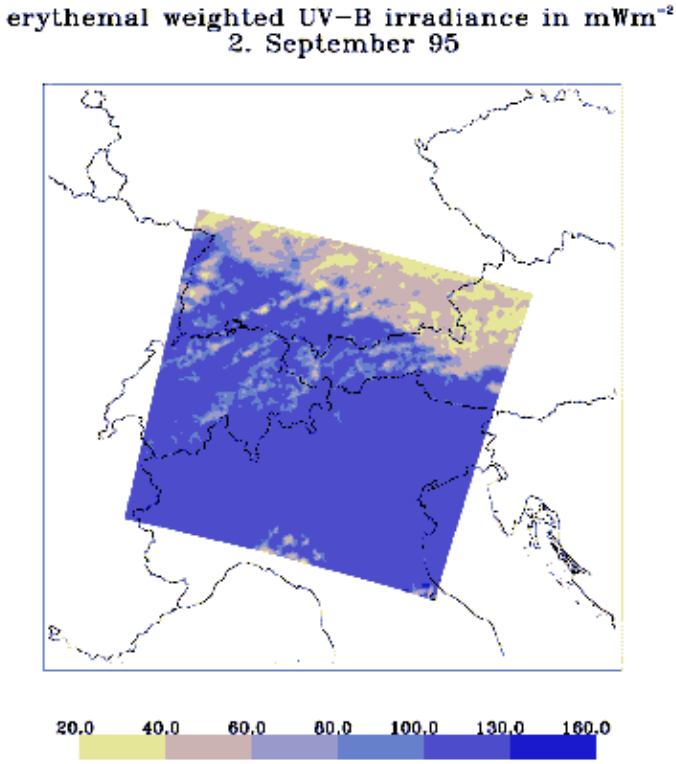

Figure 5: Distribution of surface UV-B radiation on 2. 9. 1995 calculated from GOME and ATSR-2 data. UV-B irradiances corresponding to 250 m above sea level.

4. CONCLUSIONS

The potential of the combined retrieval from simultaneous GOME and ATSR-2 data has been demonstrated for cloud detection, aerosol retrieval and surface UV-B calculation. However, further sensitivity studies and improvements of the methods are necessary. Their synergistic application will be enhanced. The cloud detection requires an improvement of the snow/ice detection. For the retrieved aerosol type error bounds need to be established which allow an assessment of the ambiguity of its solution in the light of measurement and simulation errors. For the UV-B calculation the retrieved aerosol optical depths will be used as next enhancement. One major task is the validation of each retrieval result (cloud and aerosol parameters) and derived quantities (UV-B).

5. ACKNOWLEDGEMENTS

The GOME and ATSR-2 data products used to produce the results presented in this paper are courtesy of ESA.

6. REFERENCES

Arking, A. 1991, The radiative effects of clouds and their impact on climate, *Bull. Am. Met. Soc.*, 71, 795

Armstrong, B. K. 1993, Implications of increased solar UVB for cancer incidence, NATO ASI Series, Vol. I 8, The Role of the Stratosphere in Global Ghange, Edited by M. L. Chanin, Springer-Verlag Berlin Heidelberg, 517-540

Blumthaler, M. and W. Ambach 1990, Indication of increasing solar ultraviolet-B radiation flux in alpine regions, *Science*, 248, 206-208

Caldwell, M. M. and S. D. Flint 1993, Implications of increased solar UVB for terrestrial vegetation, NATO ASI Series, Vol. I 8, The Role of the Stratosphere in Global Ghange, Edited by M. L. Chanin, Springer-Verlag Berlin Heidelberg, 495-516

Cess, R.D., Potter, G.L., Blanchet, J. P., Boer, G. J., Ghali, S. J., Kiehl, T., Le Treut, H., Li, Z. X., Liang, X. Z., Mitchell, J. F. B., Morcrette, J. J., Randall, D. A., Riches, M. R., Roeckner, E., Schlese, U., Slingo, R., Taylor, K. E., Washington, W. M., Wetherald, R. T., Yaglou, I. 1989, Interpretation of cloud climate feedback as produced by 14 general atmospheric general circulation model, *Science*, 245, 513-516

Cess, R.D., Zhang, M.H., Minnis, P., Corsetti, L., Dutton, E.L., Forgan, B. W., Garber, D. P., Gates, W. L., Hack, J. J., Harrison, E. F., Jing, X., Kiehl, J. T., Long, C. N., Morcrette, J. J., Potter, G. L., Ramanathan, V., Subasilar, B., Whitlock, C. H., Young, D. F., Zhou, Y. 1995, Absorption of solar radiation by clouds: observation versus models, Science, 267, 496

Charlson, R.J., Schwartz, S. E., Hales, J. M., Cess, R. D., Coakley, J. A., Hansen, J. E., Hofmann, D. J. 1992, Climate forcing by anthropogenic aerosols, *Science*, 255, 423-430

Correl, D. L., C. O. Clark, B. Goldberg, V. R. Goodrich, D. R. Hayes Jr, W. H. Klein, and W. D. Schecher 1992, Spectral ultraviolet-B radiation fluxes at the earth's surface: long-term variations at 39° N, 77° W, *J. Geoph. Res.*, 97, 7579-7591

De Fabo, E. C. and F. P. Noonan 1993, Ultraviolet-induced immune suppression and its relationship to stratospheric ozone depletion, NATO ASI Series, Vol. I 8, The Role of the Stratosphere in Global Ghange, Edited by M. L. Chanin, Springer-Verlag Berlin Heidelberg, 541-557

Gesell, G. 1989, An Algorithm for Snow and Ice Detection using AVHRR data: An Extension to the APOLLO Software Package, *Int. J. Rem. Sens*., 10, 897-905

Hansen, J.E., and Lacis, A. A. 1990, Sun and dust versus greenhouse gases: an assessment of their relative role in global climate changes, *Nature*, 346, 713-719

Herman, J. R., P. K. Barthia, J. Ziemke, Z. Ahmad, and D. Larko 1996, UV-B increases (1979-1992) from decreases in total ozone, *Geophys. Res. Lett.*, 16, 123-150

Hess, M. 1997, Optical properties of aerosols and clouds, submitted to *J. Geophys. Res.*

IPCC (Intergovermental Panel on Climate Change) 1992, Climate Change: the 1990 and 1992 IPCC assessments, WMO/UNEP, June

IPCC (Intergovermental Panel on Climate Change) 1995, Climate Change 1994, Cambridge Univ. Press

Kaufmann, Y. J., Fraser, R. S., Ferrante, R. A. 1991, Fossil fuel and biomass burning effect on climate - heating or cooling?; *J. Climate*, 4, 578-588

King, M.D., Kaufman, Y.J., Menzel, W.P., Tanre, D., 1992, Remote sensing of cloud, aerosol and water vapor properties from Moderate Resolution Imaging Spectrometer (MODIS). *IEEE Trans. Geosci. Rem. Sens.*, 30, 2-27

Kneizys, F. X., Shettle, E. P., Abreu, L. W., Chetwynd, J. H., Anderson, G. P., Gallery, W. O., Selby, J. E. A., Clough, S. A. 1988, User Guide to Lowtran 7, AFGL-TR-88-0177

Kriebel, K. T., Saunders, R. W., Gesell, G. 1989, Optical Properties of Clouds Derived from Fully Cloudy AVHRR pixels, *Beitr. Phys. Atmos.*, 62, 165-171

Lubin, D. and E. H. Jensen 1995, Effects of clouds and stratospheric ozone depletion on ultraviolet radiation trends, *Nature*, 377, 710-713

Madronich, S., L. O. Bjorn, M. Ilyas, and M. M. Caldwell 1992, Changes in biologically active ultraviolett radiation reaching the earth's surface, UV-B Monitoring Workshop: A Review of the Science and Status of Measuring and Monitoring Programs, March 1992, Washington D.C., C45-C57

McKinlay, A. F. and B. L. Diffey 1987, A reference spectrum for ultraviolet induced erythema in human skin, CIE Research Note, 6, 17-22

Nagel, M. R., Quenzel, H., Kweta, W., Wendling, P. 1978, Daylight Illumination-Color-Contrast-Tables, New York, Academic Press

Plass, G. N., G. W. Kattawar, and F. E. Catchings 1973, Matrix-Operator-Theory of radiative transfer, *Appl. Opt*., 12, 314-329

Popp, Th. 1993, Korrektur der atmosphärischen Maskierung zur Bestimmung der spektralen Albedo von Landoberflächen aus Satellitenmessungen, Dissertation, Universität München

Popp, Th. 1995, Correcting atmospheric masking to retrieve the spectral albedo of land surfaces from satellite, *Int. J. Rem Sens.*, 16, 3483-3508

Ramanathan, V., Barkstrom, B. R., Harrison, E. F. 1989, Climate and earth's radiation budget, *Physics Today*, 42, 22-32

Rao, C.N.R., Stowe, L.L., McClain, E.P. 1989, Remote Sensing of aerosols over the oceans using AVHRR data: Theory, practice and applications, *Int. J. Rem. Sens.*, 10, 743-749

Saunders, R. W., Kriebel, K. T. 1988, An Improved Method for Detecting Clear-Sky and Cloudy Radiances from AVHRR-data, *Int. J. Rem. Sens*., 9, 123-150

Schlichter, D., Kriebel K. T., Wendling P., Piesik B., Popp Th. 1994, PAGODA - Project for ATSR and GOME Data Application, Proposal for ESA ERS-2 AO, DLR, Oberpfaffenhofen

Smith, R.C. 1993, Implications of increased solar UVB for aquatic ecosystems, NATO ASI Series, Vol. I 8, The Role of the Stratosphere in Global Ghange, Edited by M. L. Chanin, Springer-Verlag Berlin Heidelberg, 473-493

Stolarski, R. S., P. Bloomfield, R. D. McPeters, and J. R. Herman 1991, Total ozone trends deduced from Nimbus 7 TOMS data, *Geoph. Res. Lett.*, 18, 1015-1018

World Climate Program 1986, A Preliminary Cloudless Standard Atmosphere for Radiation Computation, WCP-112, WMO/TD No. 24, Boulder

World Meteorological Organization (WMO) 1995, Scientific assessment of ozone depletion: 1994, Global Ozone Research and Monitoring Project, Rep. 37, Geneva